Acta Neuropathologica Communications

RESEARCH

Open Access

Human induced pluripotent stem cell-derived myotubes to model inclusion body myositis

Judith Cantó-Santos[1,2], Laura Valls-Roca[1,2], Ester Tobías[1,2], Francesc Josep García-García[1,2], Mariona Guitart-Mampel[1,2], Félix Andújar-Sánchez[1,2], Adrià Vilaseca-Capel[1,2], Anna Esteve-Codina[3,4], Beatriz Martín-Mur[3], Joan Padrosa[1,2], Emma Peruga[5], Irene Madrigal[2,5], Paula Segalés[6,7], Carmen García-Ruiz[6,7], José Carlos Fernández-Checa[6,7], Pedro J. Moreno-Lozano[1,2], Albert Selva O'Callaghan[8], Ana Sevilla[9,10*], José César Milisenda[1,2*] and Glòria Garrabou[1,2*]

Abstract

Inclusion body myositis (IBM) is an inflammatory myopathy that displays proximal and distal muscle weakness. At the histopathological level, the muscles of IBM patients show inflammatory infiltrates, rimmed vacuoles and mitochondrial changes. The etiology of IBM remains unknown, and there is a lack of validated disease models, biomarkers and effective treatments. To contribute to unveil disease underpins we developed a cell model based on myotubes derived from induced pluripotent stem cells (iPSC-myotubes) from IBM patients and compared the molecular phenotype vs. age and sex-paired controls ($n=3$ IBM and 4 CTL). We evaluated protein histological findings and the gene expression profile by mRNA-seq, alongside functional analysis of inflammation, degeneration and mitochondrial function. Briefly, IBM iPSC-myotubes replicated relevant muscle histopathology features of IBM, including aberrant expression of HLA, TDP-43 and COX markers. mRNA seq analysis identified 1007 differentially expressed genes (DEGs) (p-value adj < 0.01; 789 upregulated and 218 downregulated), associated with myopathy, muscle structure and developmental changes. Among these, 1 DEG was related to inflammation, 28 to autophagy and 28 to mitochondria. At the functional level, inflammation was similar between the IBM and CTL groups under basal conditions (mean cytokine expression in IBM 4.6 ± 1.4 vs. 6.7 ± 3.4 in CTL), but increased in IBM iPSC-myotubes after lipopolysaccharide treatment (72.5 ± 21.8 in IBM vs. 13.0 ± 6.7 in CTL). Additionally, autophagy was disturbed, with 40.14% reduction in autophagy mediators. Mitochondrial dysfunction was strongly manifested, showing a conserved respiratory profile and antioxidant capacity, but a 56.33% lower cytochrome c oxidase/citrate synthase ratio and a 66.59% increase in lactate secretion. Overall, these findings support patient-derived iPSC-myotubes as a relevant model for IBM, reflecting the main muscle hallmarks, including inflammation, autophagy dysfunction and mitochondrial alterations at transcriptomic, protein and functional levels.

*Correspondence:
Ana Sevilla
anasevilla@ub.edu
José César Milisenda
jcmilise@clinic.cat
Glòria Garrabou
garrabou@clinic.cat

Full list of author information is available at the end of the article

Summary
Transcriptomic and functional validation of iPSC-derived myotubes from IBM patients revealed that they displayed the main hallmarks of the disease.

Keywords Inclusion body myositis (IBM), iPSC, Myotubes, Inflammation, Autophagy, Mitochondria

Introduction

Inclusion body myositis (IBM) is an inflammatory myopathy with proximal and distal muscle weakness [32]. The prevalence ranges from 45 to 180 per million in the population over 50 years old, which is on average the age of onset [32]. Clinically, muscle weakness starts in the quadriceps and finger flexors, often with dysphagia [27]. It affects forearm muscles, leg extensors and ankle dorsiflexors [27]. Diagnosis requires muscle histology, revealing inflammatory infiltrates of CD8 + T cells and abnormal MHC-I expression; degenerative changes including rimmed vacuoles, and mitochondrial abnormalities such as ragged red fibers, cytochrome c oxidase (COX) negative cells and succinate dehydrogenase positive fibers [12, 22, 26, 47].

Unlike other idiopathic inflammatory myopathies treated with corticoids, IBM lacks effective treatment despite ongoing trials [10, 32]. IBM's cause is unknown, lacking validated models and biomarkers [10, 22, 23]. The invasive nature of the target tissue presents challenges in acquiring the ample amount of muscle tissue required for comprehensive molecular profiling of the disease, for establishing disease models and for potential biomarker or treatment discoveries [48]. Indeed, developing disease models that manifest all or some of the pathological mechanisms of the disease has been challenging, and most of them showed caveats that handicap its use to for the better understanding of disease etiology, the identification of potential biomarkers and the development of new therapeutic strategies [41].

Previous attempts to develop disease models for IBM were based on mouse and cell models. Mouse models for IBM included the MCKAβPP model [23], the VCP-mutant model and the IBM xenograft model [9]. The MCK-AβPP transgenic mouse model, based on the over-expression of AβPP in skeletal muscle [42], failed to reproduce specific histological features of IBM [23].The VCP mutant mouse, from the monogenic disease inclusion body myopathy, was confused with IBM because of its degenerative features [1, 9, 23] but lacked the inflammatory component crucial to IBM [37].The IBM mouse xenograft model was developed with the transplantation of human muscle biopsies from IBM patients into nude mice [9]. It mimicked the inflammatory and degenerative hallmarks of IBM, including endomysial inflammation, invasion of myofibers by CD3 + T cells, COX- fibers, and MyoKD or rimmed vacuoles [9, 37]. Unfortunately, mouse models could add confounding factors to the disease, thereby adding unknown bias [41].

Cell models derived from IBM patients were developed from primary myoblasts, dermal fibroblasts and lymphocytes [10, 13, 33]. Myoblasts from IBM patients reproduced degenerative changes in IBM, such as vacuolization, reduced activity of lysosomal enzymes, increased Ab42 oligomers and y-secretase activity after inhibiting the autophagic process [33]. In another study, primary myoblasts from IBM patients' muscle biopsies exposed to IL-1b and IFN-g for 24–72 h overexpressed APP and accumulated b-amyloid [39], displaying co-localization of pro-inflammatory cytokines and degenerative markers in IBM muscle [39]. However, obtaining primary myoblasts requires an invasive approach, the amount of biological material obtained is limited, and they have a brief lifespan, as they become senescent after limited rounds of division.

Fibroblasts, obtained from skin punch biopsy, also displayed inflammatory, degenerative and mitochondrial pathways related to the IBM features in muscle [10]. Besides IBM, fibroblasts are essential in the diagnosis of some degenerative and mitochondrial diseases [2, 21, 45]. In the case of lymphocytes, they also displayed mitochondrial defects, specifically related to COX/CS, showing some IBM alterations are present systemically and not only specific to muscle [13]. Nevertheless, cells obtained from primary tissues become senescent after some passages, impeding experimental assays and biobanking in the long term. Additionally, some specific features are only displayed in muscle cells.

To overcome these limitations, patient-derived induced pluripotent stem cells (iPSC) have been proposed for drug discovery, disease modeling and regenerative medicine, since they can be differentiated into muscle stripes conserving patients' characteristics and have unlimited cell passages. To differentiate iPSC to muscle cells, two methodologies have been developed: one based on the overexpression of myogenic transcription factors in the iPSCs, generally MyoD, Pax3 and Pax7, using integrative vectors such as lentivirus [28]. This method was effective, but integrative vectors could trigger genotoxicity. The second method was based on supplementation with defined factors for myogenic induction in iPSCs, trying to mimic embryonic development [15]. This approach allows the use of differentiated cells for therapeutic applications [34]. The differentiation protocols from iPSC to muscle cells are effective, as they show iPSC derived

myotubes preferentially expressing myosin heavy-chain isoforms (associated with slow and oxidative muscles) rather than developmental myosins, thus indicating postnatal composition [24] and mature muscle function in these cell models. However, while iPSC-myotubes have been developed for muscle diseases like Duchenne muscular dystrophy (DMD) [14, 30, 31] and facioscapulohumeral muscular dystrophy (FSHD) [11], their potential in IBM remains unexplored.

Due to the limitations of currently developed models of disease in IBM, and iPSCs' potential for accurate muscle cell differentiation, we hypothesized that iPSC-derived myotubes could aid in revealing IBM etiology, biomarker or therapeutic discovery. Thus, in this proof-of-concept study, IBM patients vs. CTLs iPSCs were developed, characterized, differentiated into myotubes and phenotyped (by RNAseq, protein and functional means) to check if they displayed the IBM muscle hallmarks, including inflammation, degeneration and mitochondrial changes, thus becoming a potential cell model for IBM.

Materials and methods

Study design and sample inclusion

A case-control study was conducted from 2018 to 2022 in the Department of Internal Medicine at the Hospital Clínic of Barcelona (Barcelona, Spain), including 3 patients (IBM) and 4 age and sex-paired healthy volunteers (CTL) (Table 1). IBM patients were diagnosed according to Lloyd's criteria [26]. All participants signed the informed consent approved by the Ethical Committee of our hospital (code HCB/2019/0558).

Skin biopsies from IBM patients and CTL were seeded to obtain fibroblasts, further reprogrammed into iPSCs. iPSCs' pluripotency was validated following standard tests (Fig. 1) and cells were later differentiated into myotubes. iPSC-myotubes were phenotyped by RNA-seq, protein expression and functional assays to detect potential inflammatory, autophagic and mitochondrial changes.

Generation of iPSC

Cell reprogramming

Fibroblasts from skin punch biopsies were cultured in 5 mM glucose DMEM supplemented with 10% FBS and 1% penicillin-streptomycin, at 37 ∘C, 5% CO_2 air incubator (all from Gibco, Waltham, MA, USA). Peripheral blood mononuclear cells (PBMCs) were isolated from total blood using the Lymphoprep™ (#07801, Stemcell, Vancouver, Canada) density gradient. Fibroblasts at passage 4 and PBMCs were transduced with the Cytotune_iPS 2.0 Sendai Reprogramming kit (A16518, ThermoFisher Scientific, Waltham, MA, USA) following the manufacturer's instructions. Isolated iPSCs were cultured on Geltrex (A1413202, Gibco, Waltham, MA, USA) pre-coated 6-well plates in mTeSR1 (85850, StemCell Technologies, Vancouver, BC, Canada). All the iPSC lines were passaged to passage 12 or higher with TrypLE Express (12604013, Gibco Waltham, MA, USA) for full characterization (Supplementary Tables 1 and 2).

Pluripotency validation

Staining of alkaline phosphatase activity (Abcam 242286) and immunofluorescence of OCT4 and NANOG (Supplementary Table 3) were performed in iPSC lines under the Zoe Fluorescent Cell Imager (Bio-Rad). qRT-PCR was performed on the iCycler (Bio-Rad), Fast SYBR Green Master Mix (Bio-Rad) and specific primers (Supplementary Table 3) were used to quantify the expression of endogenous *OCT4*, *SOX2*, and *NANOG*, normalized with *GAPDH* and relative fold change with respect to the iPSCs (Fig. 2d and Supplementary Fig. 1d).

Table 1 Clinical data of the cohorts and features from IBM patients muscle's biopsies

Sample code	Sex	Age	Time symptoms to diagnosis (months)	Rimmed Vacuoles	Inflammation	MHC1	Auto Ab	CD57	Mitochondrial Changes	IBMFRS	Evolution
IBM1	F	83	12	+	+++	NA	All -	T clonal	YES +	8	Progressive
IBM2	M	78	12	+++	+++	+ not universal	All -	NA	NO	28	Progressive
IBM3	M	63	36	+	+++	Universal	All -	NA	YES +	27	Progressive
CTL1	M	69									
CTL2	F	52									
CTL3	M	40									
CTL4	F	61									

Abbreviations: IBM: Inclusion body myositis patients; CTL: healthy control subjects; Sex: F:female; M:male; Rimmed vacuoles: from 0 to +++; Inflammation: from 0 to +++; MHC1: Major Histocompatibility Complex: Universal; NA: not available; + not universal: splattered pattern; Auto Ab: Autoantibodies: Myositis specific and associated auto antibodies include: Anti-Jo-1, anti-SRP, anti-Mi2, anti-TIF1gamma, anti-MDA5, anti-SAE, anti-NXP2 and anti-HMGCR (specific) and anti-PM/Scl, anti-Ro, anti-La, and anti-U1RNP (associated); Mitochondrial changes: Yes or No. Yes: RRF and/or COX neg. Yes + (strong alterations). NO: no changes; Age and gender-paired distribution between cohorts (p = NS). IBMFRS: Inclusion Body Myositis Functional Rating Scale (from 0 -inability- to 40 points -health-); Evolution: Progressive vs. stable phase of the disease

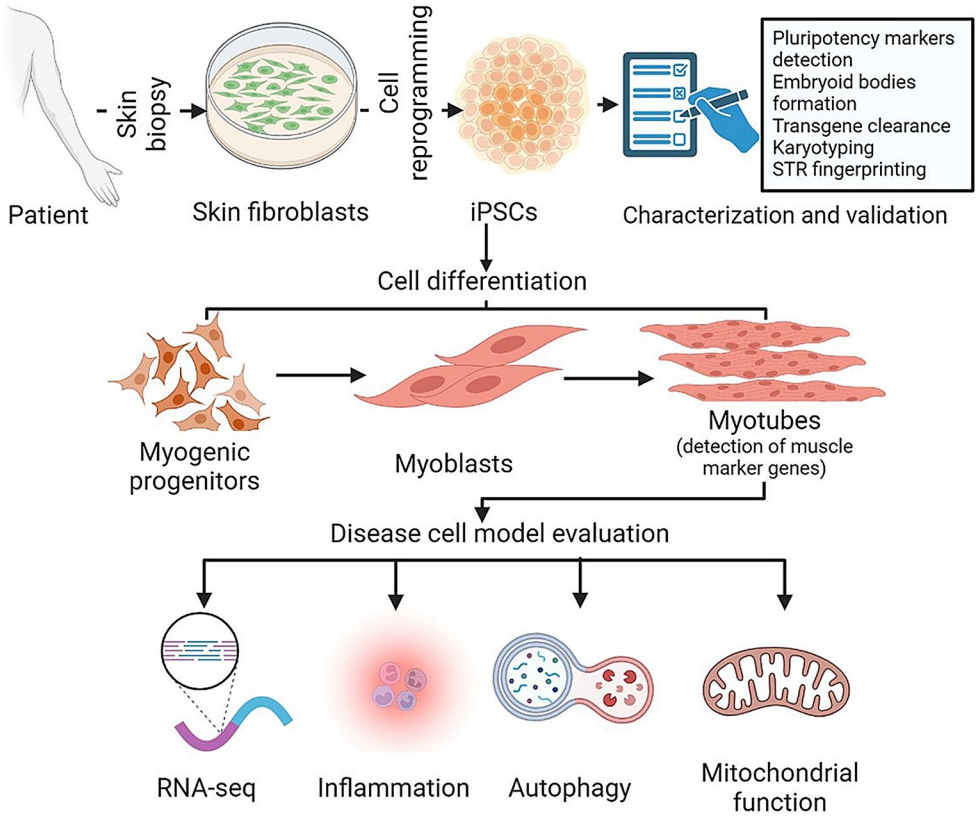

Fig. 1 Flowchart: Obtaining iPSCs from fibroblasts and differentiation into muscle cells. First, a skin biopsy is taken from IBM patients and CTLs and fibroblasts grow. Fibroblasts are reprogrammed into iPSCs, which are characterized to validate their pluripotency. Afterwards, iPSCs are differentiated into muscle cells, from myogenic progenitors to myoblasts and then to myotubes. iPSC-derived myotubes are phenotyped by RNA-seq, protein and functional analysis (inflammation, autophagy and mitochondrial function) to examine if they are an appropriate disease model for IBM. Abbreviations: iPSCs: induced pluripotent stem cells; IBM: inclusion body myositis; CTL: healthy individuals. This figure was created with Biorender.com

Three germ layer differentiation

Spontaneous differentiation to embryoid bodies (EB) started with iPSCs dissociation and transfer to low attachment 96-well plates (Costar, Corning) (40,000 cells per well) in Knockout DMEM supplemented with 20% Knockout serum replacement, non-essential amino acids, L-glutamine, penicillin/streptomycin (all from Thermo Fisher Scientific), b-mercaptoethanol (Sigma-Aldrich) and 10 µM of thiazovivin or Rock inhibitor (S1049, Selleck, Houston, TX, USA). Cell aggregates (EBs) were cultured for 16 days. mRNA was extracted using the RNeasy Micro kit (Qiagen), 1 µg was reversely transcribed with the High-Capacity cDNA Reverse transcription kit (Applied Biosystems) and cDNA was used for qPCR (see Supplementary Table 3 for oligo sequences) (Fig. 2d and Supplementary Fig. 1d). Some EBs were transferred to geltrex-precoated for immunostaining (at day 8 and kept in monolayer culture until day 16) of the three lineage markers (*SOX17* (endoderm), *TUJ1* (ectoderm) and *SMA* (mesoderm) markers (Fig. 2c, Supplementary Fig. 1c)).

FACS analysis

Flow cytometry was performed to detect SSEA-4, TRA 1–60 and TRA 1–81 pluripotency markers (Supplementary Fig. 2a), acquired on a FACS Canto II flow cytometer equipped with FACS Diva analysis software (Becton Dickinson, San Jose, CA, USA).

DNA Fingerprinting analysis (Short Tandem Repeats (STR) analysis)

16 highly polymorphic STR sequences of DNA were analyzed using the AmpFlSTR® Identifiler® Plus PCR Amplification Kit and GeneMapper ID software (Applied Biosystems) in fibroblasts and PBMCs (before reprogramming) and iPSCs (Supplementary Table 2).

Transgene-free confirmation

Total RNA was extracted from iPSCs with the RNeasy Mini Kit (Qiagen) and reversely transcribed with the High-Capacity cDNA Reverse Transcription Kit (Applied Biosystems). The cDNA was amplified by PCR with MyFi DNA Polymerase (Bioline) under specific primers against OSKM factors (primer sequences in Supplementary Table 3).

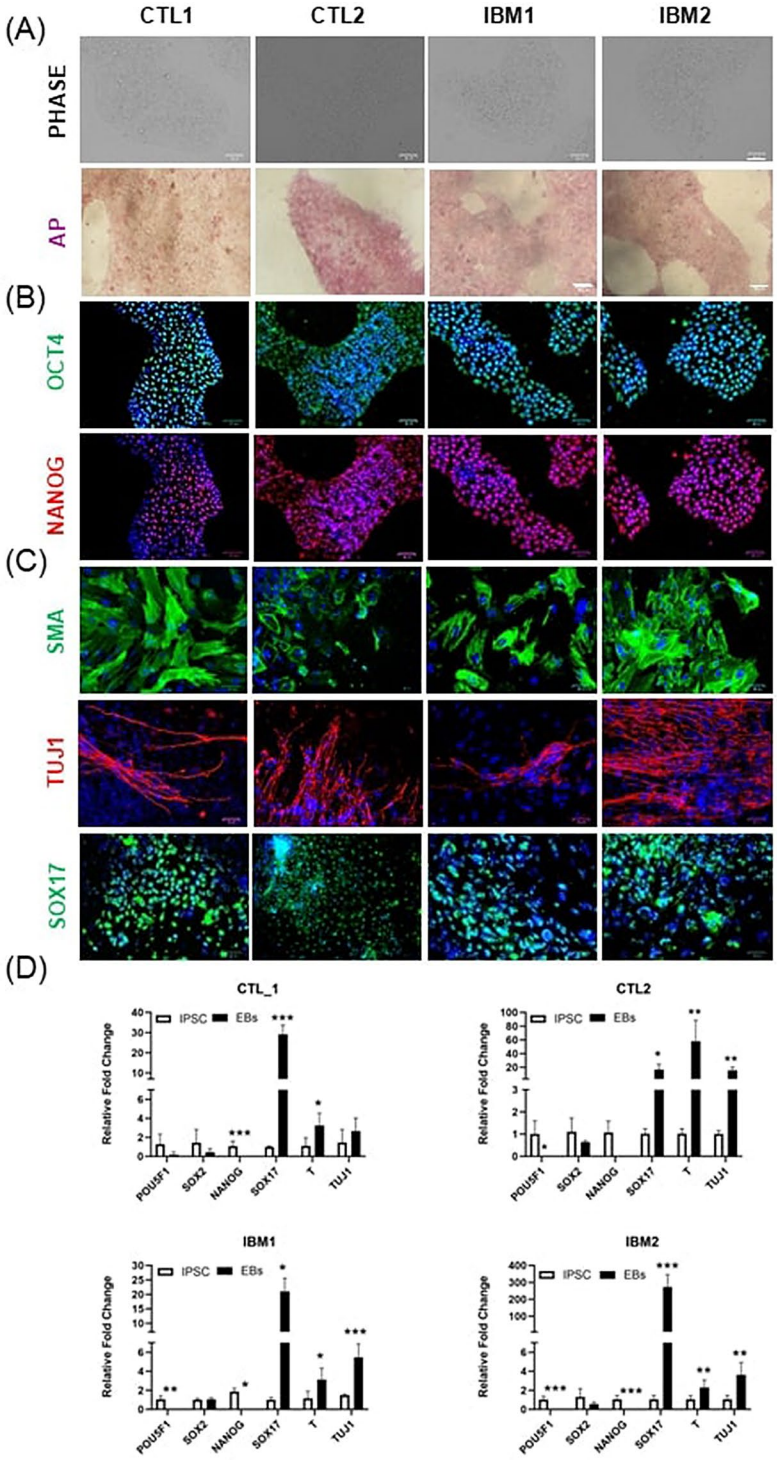

Fig. 2 Characterization of 2 IBM and 2 CTL iPSC lines. **A** Phase contrast and alkaline phosphatase images. Scale bar: 200 µM. **B** Immunodetection of pluripotency markers OCT4 and NANOG. Scale bar: 200 mm. **C** Expression of the three germ layer markers by immunofluorescence analysis of in vitro embryoid body differentiation cell cultures using specific antibodies against the endodermal marker SOX17, the mesodermal marker SMA, and the ectodermal marker TUJ1. Nuclei were stained with DAPI. Scale bar: 100 mm. **D** Expression levels of pluripotency genes (*POU5F1*, *SOX2*, *NANOG*) and early lineage markers (*SOX17*, *T*, *TUJ1*) determined by real-time PCR in the iPSC lines and in those same lines differentiated into embryoid bodies. These tests leaded to the validation of the pluripotency in the iPSC lines. The characterization of the other IBM and CTL lines is represented in Supplementary Fig. 1

Mycoplasma detection

Endpoint PCR using mycoplasma-specific primers (in Supplementary Table 3) and iPSC cell culture supernatants was used to detect the absence of mycoplasma.

Karyotype analysis

The karyotype of the reprogrammed iPSC lines was done by the Molecular Genetic section (Hospital Clinic of Barcelona) around passage 15. Twenty G-banded metaphase cells per sample were analyzed by cytogenetic analysis and displayed a standard female or male karyotype (Supplementary Fig. 2b).

Obtaining iPSC-derived myotubes

iPSC differentiation to myotubes using growth factors

The Genea Biocells skeletal muscle differentiation kit (SKM-KIT, San Diego, CA, USA) [11] was used to differentiate iPSCs into myotubes, following the manufacturer's protocol. Characterization and functional experiments were performed on myotubes on day 7. Each differentiation was performed three times per sample.

Characterization of iPSC-derived myotubes with qPCR and immunofluorescence of muscle-associated markers

iPSC-myotubes were stained with sarcomeric anti-α-actinin (A7811 Millipore Sigma, Burlington, MA, USA) and Alexa Fluor 488 donkey anti-mouse IgG antibody (Invitrogen A-21202, Life Sciences Europe, NL), counterstaining with DAPI. Images were obtained with a Zeiss LSM 880 laser scanning confocal system using a 63X oil immersion objective.

GoTaq® qPCR Master Mix (A6001, Madison, WI, USA) and specific primers (Supplementary Table 3) were used to quantify the expression of *DESMIN*, *MYOD*, *MYOG*, and *MHC-I* at day 7 in iPSC-myotubes, normalized with GAPDH as an internal control.

Phenotyping iPSC-derived myotubes for IBM muscle hallmarks

RNA extraction and mRNA library preparation and sequencing

Total RNA was isolated from cell lysates of 3 IBM and 3 CTL iPSC-myotubes. Libraries were prepared and sequenced on the HiSeq 4000 (Illumina) with a read length of 2 × 51 bp using the HiSeq 4000 SBS kit (Illumina), followed by primary data analysis and the generation of FASTQ sequence files. Additional information is provided in the Supporting information.

RNA-seq data processing and analysis

RNA-seq reads were mapped against the human reference genome (GRCh38). Differential expression analysis, gene ontology enrichment analysis, and gene set enrichment analysis (GSEA) were performed. The Pathcards database [4], Gene a la Cart [19], Mitocarta 3.0 [38], Muscle Gene Table [20], Autophagy [6] and Development [49] gene lists were used to relate differentially expressed genes (DEGs) to the pathways of interest. Additional information is provided in the Supporting information.

Protein detection by Western blot analysis

To examine IBM protein markers related to inflammation, degeneration and mitochondria in IBM muscle, we determined the expression of HLA class I ABC, TDP-43, COX II and COX IV in iPSC-myotubes through western blot analysis. Blots were probed against the anti-HLA class I ABC (Proteintech #15240-1-AP, Manchester, UK), anti-TDP-43 (LSBio #LS-B4521, Shirley, MA), anti-COX II (Invitrogen, #A6404, NL) and anti-COX IV (#A21347 Life Technologies, NL), using SYPRO Ruby as a loading control (Invitrogen, #S12000, NL).

Inflammatory cytokine array

The secreted cytokines in iPSC-myotubes supernatants were quantified using the Human Cytokine Antibody Array C5 (AAH-CYT-5-8, RayBio® C-Series, Atlanta, GA, USA) in basal conditions vs. treated with lipopolysaccharide (LPS) (Invitrogen, #00-4976, NL) for 24 h at 100 ng/ml. Supernatants were collected after 48 h with cell media, in the case of LPS exposure, we collected them 24 h in after LPS exposure, plus 24 h in cell culture media.

Collected supernatants were loaded into the Human Cytokine Antibody Array C5 (AAH-CYT-5-8, RayBio® C-Series, Atlanta, GA, USA). Cytokines were detected by chemiluminescence using the Image Quant TL Software (GE Healthcare) and calculated by AAH-CYT-5-8 analysis tools provided by RayBiotech, Inc. (Atlanta, USA). We considered the cytokines with an expression in basal and treated conditions higher than 0 (the rest were not expressed in iPSC-myotubes). The results were normalized by the cell count per supernatant and compared between basal vs. LPS treatment in IBM vs. CTL iPSC-myotubes.

Immunofluorescence for autophagosome characterization

Autophagosomes were stained in basal vs. bafilomycin A1 treatment conditions in each sample. Bafilomycin A1 treatment (100 nM, from *Streptomyces griseus* (Sigma-Aldrich® #B1793 SIGMA, Missouri, USA) for 6 h) blocks the degradation of autophagolysosomes. Autophagosomes were stained with anti-LC3 pAB (MBL International® #PM036, Massachusetts, USA) and donkey anti-rabbit Alexa Fluor® 488 IgG antibody (Life Technologies Europe, NL), counterstaining with DAPI. Images were obtained with a Zeiss LSM 880 laser scanning confocal system using a 63X oil immersion objective.

Autophagy protein array

Two cell lysates were obtained from each IBM and CTL iPSC-myotube sample. One lysate was obtained under basal conditions and the other at 6 h under 10 nm bafilomycin A1 treatment (B1793, Sigma, Burlignton, MA, USA). Each lysate (250 µg of protein) was loaded in the RayBio® C Series Human Autophagy Array 1 (Cat#: AAHATG-1-8, RayBiotech, Inc., Atlanta, GA, USA), incubated overnight at 4ºC, detected by chemiluminescence using the Image Quant TL Software (GE Healthcare), and calculated by the AAH-ATG-1 analysis tools provided by RayBiotech, Inc. (Atlanta, USA).

Mitochondrial respiration

Mitochondrial respiration was measured by the oxygen consumption of the mitochondrial respiratory chain (MRC), detected with the XF Cell Mito Stress Test™ (Seahorse-XFe24-Analyzer, Agilent Technologies), according to the manufacturer's protocol, and normalized by the protein content per sample.

Total antioxidant capacity (TAC)

TAC was measured in 100 µL of iPSC-myotubes supernatants (at day 7) after 72 h in culture using an OxiSelect™ Total Antioxidant Capacity Assay kit (Cell Biolabs Inc., San Diego, CA, USA) by spectrophotometry at 490 nm and normalized by cell count (µM CRE (Copper Reducing Equivalents)).

MRC enzymatic activities: cytochrome c oxidase (COX) and citrate synthase (CS) functions

COX and CS enzymatic activities were measured spectrophotometrically in 40 µg of total protein per myotube's sample according to standardized protocols [13].

Lactate secretion

Lactate was quantified in 100 µL of myotubes' supernatants (at day 7) after 72 h in culture, with the epoc® Blood Analysis System (epoc System Software version 3.32.0, Siemens Healthineers Global, Erlangen, Germany). The lactate concentration was normalized by cell count (mmol/L/cell).

Statistical analysis

Statistical analysis was performed with the Statistical Package for the Social Sciences software, version 27 (IBM SPSS Statistics; SPSS Inc.) and GraphPad Prism 9 (GraphPad Software, San Diego, CA, USA). Results were expressed as mean ± SEM or as fold change between conditions, with one data point per parameter per patient. Each data point per patient was the mean of multiple replicates (≥ 3). The obtained data were compared between independent experiments using the non-parametric Mann-Whitney U test or Kruskal-Walli's test. The significance threshold was set at a p-value < 0.05.

Results

Clinical and epidemiological data

The samples included in this study were 3 IBMs and 4 CTLs, all derived from donor samples (all fibroblasts except CTL3 (PBMCs)). Both cohorts were paired by age and sex and belonged to the white Caucasian population (Table 1). All three patients were in a progressive stage of the disease (vs. stable phases) and, according to the IBM functional rating scale (IBMFRS), that ranges from 0 (inability) to a maximal 40 threshold (health), the IBM cohort scored 8–28, suggestive of moderate clinical severity.

Generation of iPSC and differentiation into myotubes

The outline of the study was found in Fig. 1. It includes fibroblast reprogramming (and 1 PBMC sample) into iPSCs, their differentiation into myotubes, and the phenotyping of IBM hallmarks by mRNA-seq and functional studies.

First, iPSCs generation from IBM and CTL samples was performed using the transgene-free mRNA Sendai virus approach. To characterize the newly formed iPSC, we checked their pluripotency, EB formation, G-band karyotype, STR fingerprinting, mycoplasma absence and transgene clearance. Details of these data were represented in Fig. 2, in the Methods section, in Supplementary Figs. 1 and 2, and in Supplementary Tables 1, 2 and 3.

All iPSCs passed the tests except for the transgene silencing in IBM3, which kept the Sendai virus, KOS and c-Myc after multiple passages (Supplementary Fig. 1e). Moreover, in IBM3, the expression of EB markers *SOX17* (endoderm) and *T* (mesoderm) was similar than in iPSCs. As IBM3 did not display aberrant gene expression or functional alterations, it was kept in the study, as done by Mournetas et al. 2022 [31], who observed the same behavior as in the transgene-free iPSCs.

Once the iPSCs were validated, they were differentiated into skeletal muscle cells. The expression of skeletal muscle markers (*MYOG*, *MYOD*, *DESMIN* and *MHC-I* (Fig. 3a)) and positive sarcomeric anti-α-ACTININ staining in myotubes, revealed their muscle maturity (Fig. 3b).

Gene expression profile of iPSC-myotubes in IBM vs. CTL samples

The first step in the phenotyping of IBM vs. CTL iPSC-myotubes was an mRNA-seq analysis. In the principal component analysis (PCA), we observed both cohorts separated according to PC1 (Fig. 4a), clustering patients apart from controls. The heatmap represents the top 50

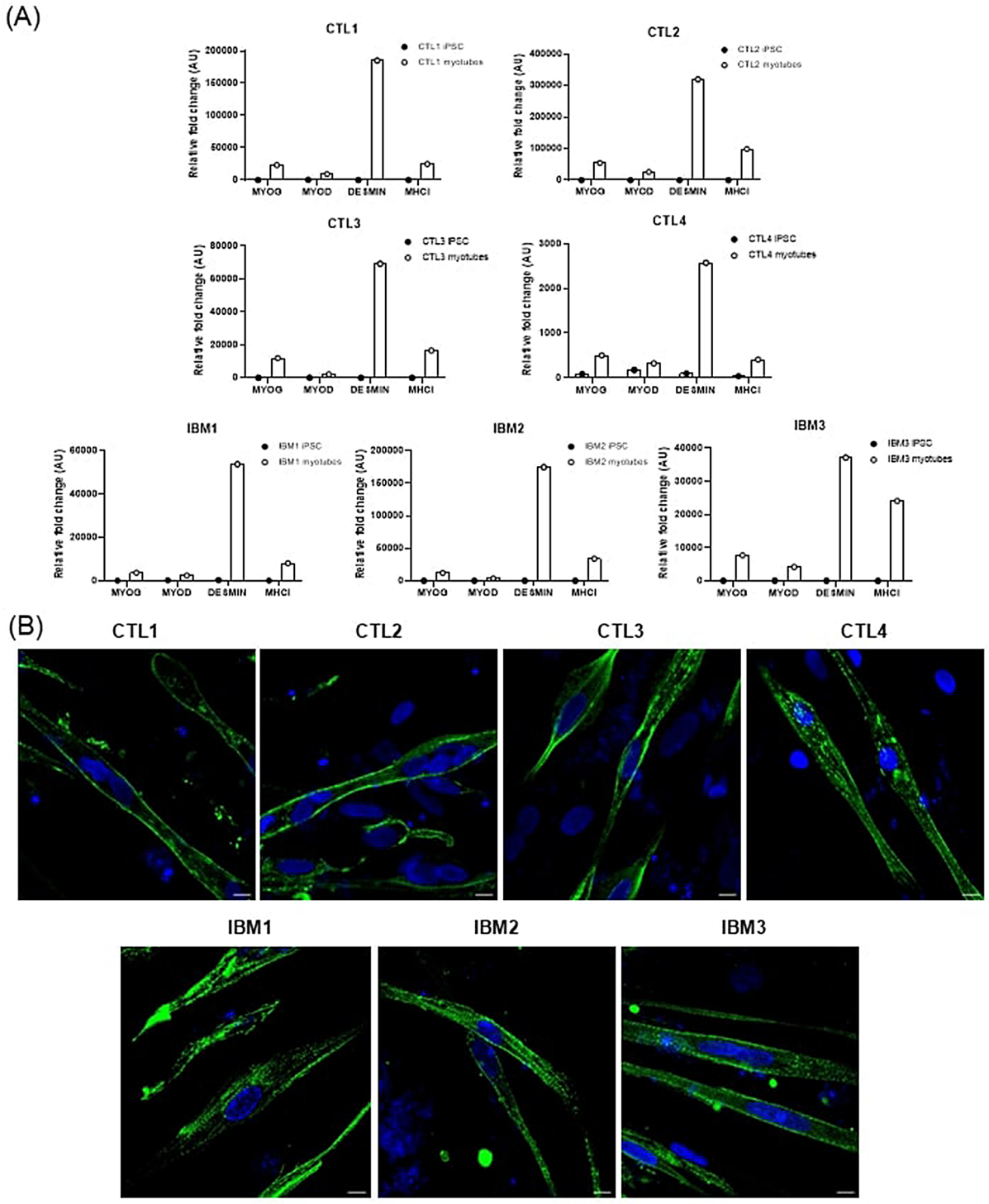

Fig. 3 Characterization of iPSC-derived myotubes in IBM vs. CTL lines. **A** Expression levels of muscle marker genes (*MYOG*, *MYOD*, *DESMIN*, and *MHCI*) determined by real-time PCR in the iPSC lines and in those same lines differentiated to myotubes. **B** Immunodetection of sarcomeric α-ACTININ. Nuclei were stained with DAPI. Scale bar: 10 µm. The positive detection of muscle markers in iPSC-myotubes confirmed iPSC lines differentiated into myotubes. IBM and CTL iPSC-myotubes displayed similar morphology and cell growth rate

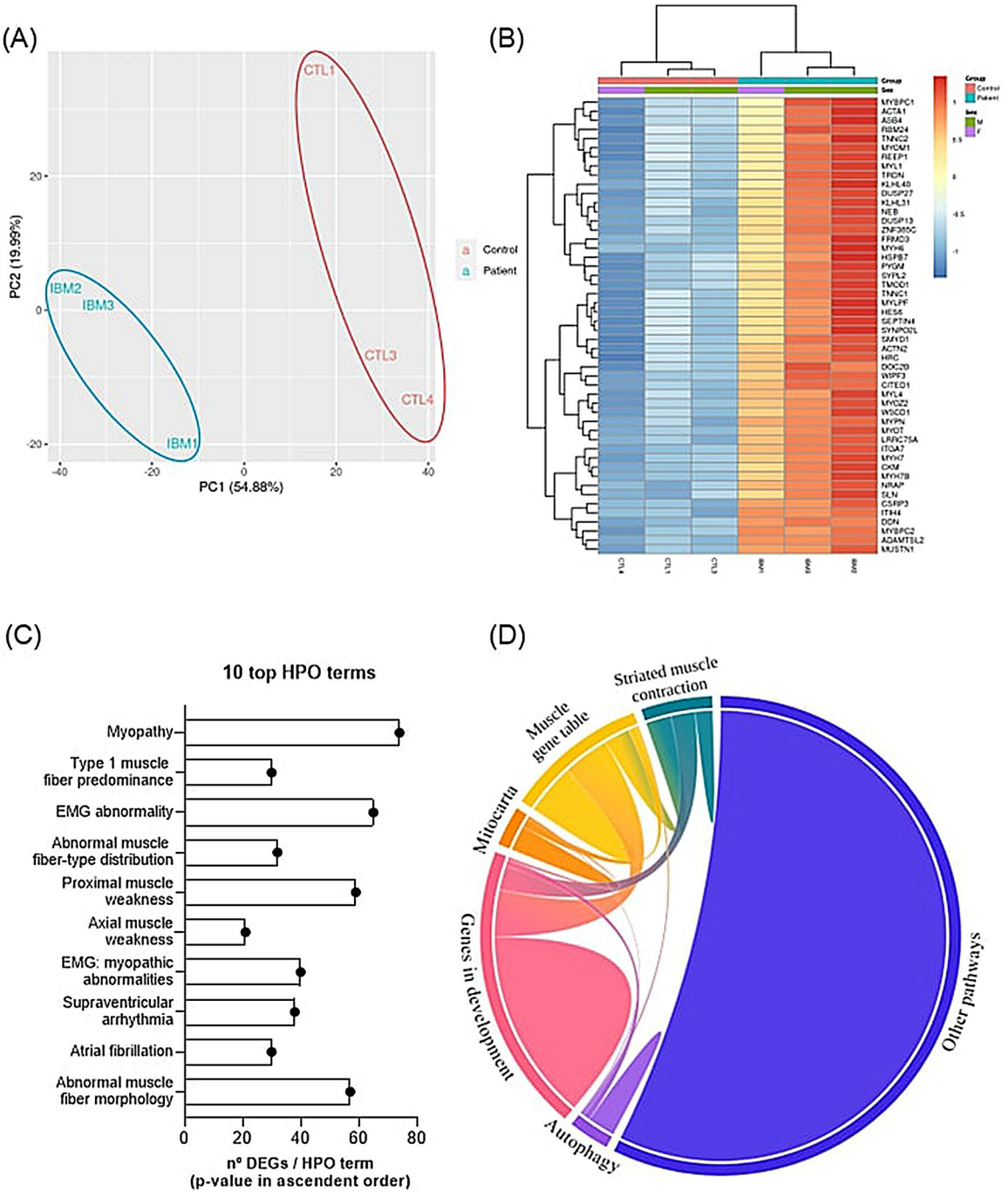

Fig. 4 RNA-seq in iPSC-derived myotubes from IBM vs. CTL lines. **A** Principal component analysis (PCA). **B** Heatmap of the top 50 differentially expressed genes (DEGs) in IBM vs. CTLs. **C** Top 10 HPO terms. **D** Chord diagram of the targeted RNA-seq analysis. Each pathway is represented by a different color. The RNA seq analysis revealed myopathic, autophagy and mitochondrial DEGs in IBM vs. CTL iPSC-myotubes

genes with the most differential expression between IBM and CTLs, all of them upregulated in IBM (Fig. 4b).

The top 50 upregulated genes in the heatmap were mostly related to muscle fiber structure and contraction (Fig. 4b). Specifically, *ACTA1*, *MYH6*, *MYOZ2*, *MYH7*, *ACTN2*, *SYNPO2L*, *MYPN* and *CSRP3* genes were associated with skeletal muscle fibers and sarcomere organization [43]. Some of them were also involved in muscle contraction (*ACTA1*, *MYH6*, *ACTN2*) together with *NEB*, *TNNC2*, *TMOD1* and *MYL4*, among other genes [43]. Some of these genes were related to late-onset distal muscle weakness (*NEB*, *ACTA1*), autophagic vacuoles (*MYOT*, *ACTA1*, *ACTN2*) and neuromuscular dysphagia (*NEB*, *ACTA1*, *MYPN*), all of which are clinical

symptoms in IBM patients [43]. In addition, 3 genes were related to other myopathies, like *MYH7* (in myosin storage myopathy), *MYOT* (in limb-girdle muscular dystrophy and myofibrillar myopathies), and *ACTA1* (nemaline myopathy and multiple congenital myopathies) [19].

In the total mRNA-seq, there were 1007 DEGs with p-value adj < 0.01 and |log2FC| ≥ 1.5 between IBM and CTL myotubes, 789 upregulated and 218 downregulated genes (Supplementary Table 4). In the gene ontology (GO) enrichment analysis, muscle structure, development and differentiation gene clusters were the most represented in the mRNA-seq, biological process (BP), cell compartment (CC) and molecular function (MF) GO databases. In the human phenotype ontology (HPO), the top HPO terms were related to myopathy, including proximal muscle weakness and abnormal muscle fiber morphology (Fig. 4c). The KEGG, Reactome and Wiki Pathways databases confirmed the findings related to altered muscle contraction and signaling.

All the DEGs, gene clusters, and pathways related to myopathy and muscle functions display clinical manifestations of IBM. For instance, when we examined those DEGs present in the Muscle Gene Table of muscular diseases [20], we found 100 DEGs, including *ACTN2*, *COL6A3* and *MYOD1*, causal genes of myopathies like distal myopathy, Bethlem myopathy, and congenital myopathy, respectively. Also, as mentioned in the heatmap, multiple DEGs were related to muscle contraction. Thus, we examined the striated muscle contraction pathway, containing 41 genes in the Pathcards database [36], and found that 28 out of 41 were deregulated in IBM vs. CTL iPSC-myotubes, confirming the altered muscle contraction in this cell model. We did the same for developmental genes [49] and found 203 DEGs matching the list in the RNA data set. All DEGs from the pathways mentioned previously were represented in Fig. 4d and listed in Supplementary Table 5.

To delve into the molecular alterations of IBM in muscle, we search specifically for the DEGs involved in inflammation, degeneration and mitochondria, listed in Supplementary Tables 5 and represented in Fig. 4d. We only found 1 DEG related to inflammation (*IL11*), revealing the absence of inflammation in the mRNA seq of these cells. However, in autophagy, we found 28 DEGs, including 2 related to amyloid precursor protein (*APP*) processing, *PAWR* and *PSEN2*, the first involved in the progression of age-related diseases, and the second causal of an inherited form of Alzheimer's disease. *BDNF*, whose expression is reduced in Alzheimer's, Parkinson's, and Huntington's disease patients, was also downregulated in this IBM group. *DEPTOR*, a negative regulator of mTORC signaling, and *MAP1LC3C*, involved in antibacterial autophagy, were upregulated. Related to mitochondrial function, 28 DEGs matched the ones in Mitocarta 3.0 [38], including *ACADS*, *ACACB* and *HSD17B8*, involved in fatty acid metabolism; *CHCHD10*, *SMDT1* and *COX6A2*, involved in mitochondrial structure and function [38, 44]. Specifically, *CHCHD10* is part of the cristae structure, *SMDT1* is in a calcium channel in the mitochondrial inner membrane, and *COX6A2* is the terminal enzyme of the MRC that catalyzes the electron transfer from cytochrome c to oxygen. *PRXL2A*, involved in redox regulation of the cell, and *CKMT2*, responsible for the transfer of high-energy phosphate from mitochondria to creatinine (the cytosolic carrier), were also among the DEGs related to Mitocarta 3.0 [38].

Overall, we found a clear deregulated pattern by mRNA seq in IBM iPSC-myotubes, displaying myopathy-related alterations together with the impairment of degeneration and mitochondrial-related genes.

Protein detection of IBM muscle pathological features in IBM iPSC-myotubes

To determine the expression of IBM muscle histopathology features at the protein level, we quantified the expression of HLA (inflammation), TDP-43 (autophagy) and COX IV and COX II (mitochondria), which aid in the diagnostic criteria of IBM. As in the muscle of IBM patients, there was an aberrant expression of HLA, TDP-43 and COX IV and COX II markers in IBM iPSC-myotubes (Fig. 5). These results confirmed a higher inflammation but reduced autophagy and mitochondrial function in iPSC-myotubes, in correspondence to histological findings characteristics of the target tissue of disease (the muscle of IBM patients).

Inflammatory Profile in IBM vs. CTL iPSC-myotubes

To examine the cytokine profile, we analyzed 80 inflammatory and regulatory cytokines in the supernatant of iPSC-myotubes in basal conditions vs. treated with LPS. The regulatory cytokines refer to those related to development, growth or differentiation.

The secreted cytokines in basal conditions displayed a slightly reduced concentration in IBM myotubes (Fig. 6a, ratio of the mean IBM vs. mean CTL concentration per cytokine < 1). However, when iPSC-myotubes were exposed to LPS, IBM myotubes showed a higher cytokine secretion than CTL (Fig. 6b).

In fact, among the top 10 secreted cytokines with LPS treatment, IL-7, GRO-α, GMCSF, MCP2, ENA78, I309, IL-10, IL-8 were all inflammatory cytokines and were among the lowest expressed in basal conditions. Briefly, IL-7 plays a role in B and T cell development; ENA-78 (CXCL5), GRO-α (CXCL1) and IL-8 (CXCL8) have a chemotactic activity for neutrophils; GMCSF is involved in the production, differentiation, and function of granulocytes and macrophages; MCP-2 (CCL8), is a chemokine for monocytes, lymphocytes, basophils and

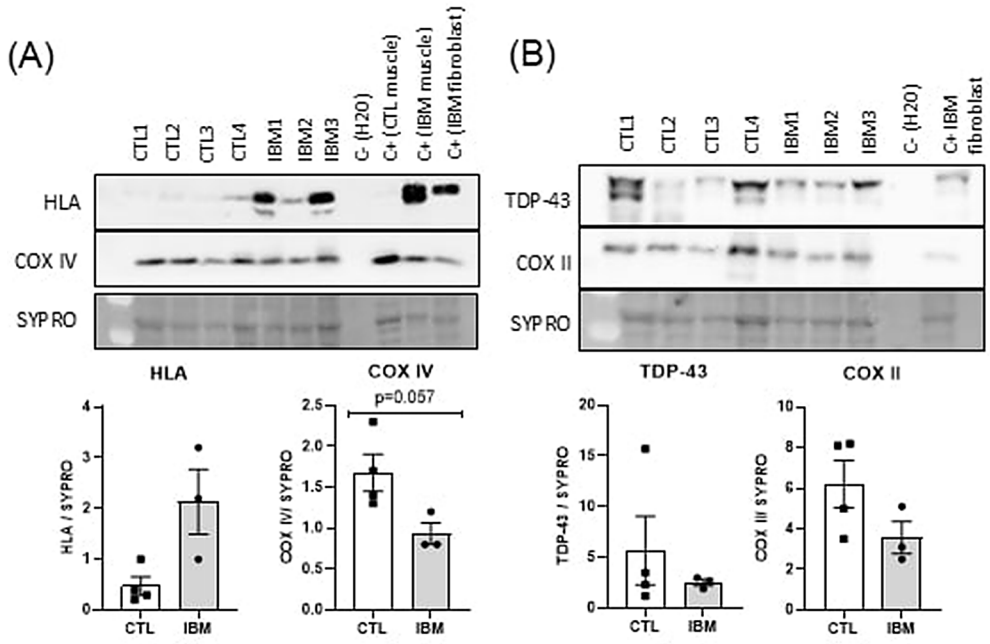

Fig. 5 Protein expression of IBM muscle pathological features in IBM iPSC-myotubes. **A** HLA and COX IV. **B** TDP-43 and COX II. All inflammatory (HLA), autophagic (TDP-43) and mitochondrial markers (COX IV and COX II) were normalized by SYPRO total protein content. Abnormal levels of HLA, TDP-43, COX IV and COX II markers in IBM iPSC-myotubes matched the features in the muscle histopathology of IBM patients, suggestive of higher inflammation and dysfunctional autophagic and mitochondrial performance

eosinophils; I309 displays chemotactic activity for monocytes but not for neutrophils; and IL-10 has with pleiotropic effects in immunoregulation and inflammation. These trends suggested that under stressful conditions, IBM iPSC-myotubes tend to increase their inflammatory response, suggesting that these IBM myotubes are more susceptible to display an inflammatory profile, as seen in the muscle of IBM patients (with higher HLA, see Fig. 5a). Thus, inflammation in IBM was increased at the protein level (Figs. 5a and 6), especially under stress, but not seen at the mRNA seq level (Fig. 4).

Autophagy variations in IBM vs. CTL iPSC-myotubes

Autophagy was analyzed in iPSC-myotubes in basal vs. treated conditions (6 h-bafilomycin A1 treatment). The accumulation of autophagosomes in basal conditions was similar in IBM vs. CTL (Fig. 7a). However, treated iPSC-myotubes displayed slightly more autophagosomes in the CTL cohort. These results suggested an impairment in IBM iPSC-myotubes related to autophagosome closure (at later stages of autophagic process).

Moreover, we checked the protein levels of 20 autophagy mediators in basal vs. treated conditions (6 h under bafilomycin A1 treatment). The representative graph (Fig. 7b) contains the ratio of basal vs. treated concentrations for each protein in the IBM vs. CTL cohorts. In IBM, the similar concentration of mediators before and after the blockage of the process displays a reduced autophagic flux, suggesting that autophagy was less active in IBM. In detail, ATG7, Beclin, LAMP1 and α-synuclein accumulation, observed in CTLs, were absent or highly reduced in IBM iPSC-myotubes. ATG7 promotes mitophagy, decreases oxidative stress, and is involved in glucose metabolism. Beclin is involved in the initiation of autophagy, endocytosis, and mitochondrial apoptosis. LAMP1 is involved in lysosome biogenesis. α-synuclein acts as a chaperone of the SNARE complex (vesicular transport of secretory components) [19, 44]. In IBM, ATG3, ATG10 and Rheb were contrarily increased. ATG3 is involved in autophagy-related cell death and mitochondrial homeostasis when bound to ATG12; Rheb activates mTORC1, which inhibits autophagy, and ATG10 participates in autophagosome formation. This reveals that in IBM, the autophagosome formation process started (high ATG10) but after that, the process was somewhere impaired or blocked, and apoptosis (ATG3) or the mTORC pathway (Rheb) reinforce the idea that autophagy was not highly activated at later stages. In CTLs, autophagy was more active, and the difference was higher when the process was blocked by bafilomycin A1, also in mitochondria (ATG7, Beclin). A lower activity of basal autophagy is often linked to senescence, so the IBM profile could suggest an accelerated aging phenotype concerning autophagy, as previously observed by LC3-immunofluorescence.

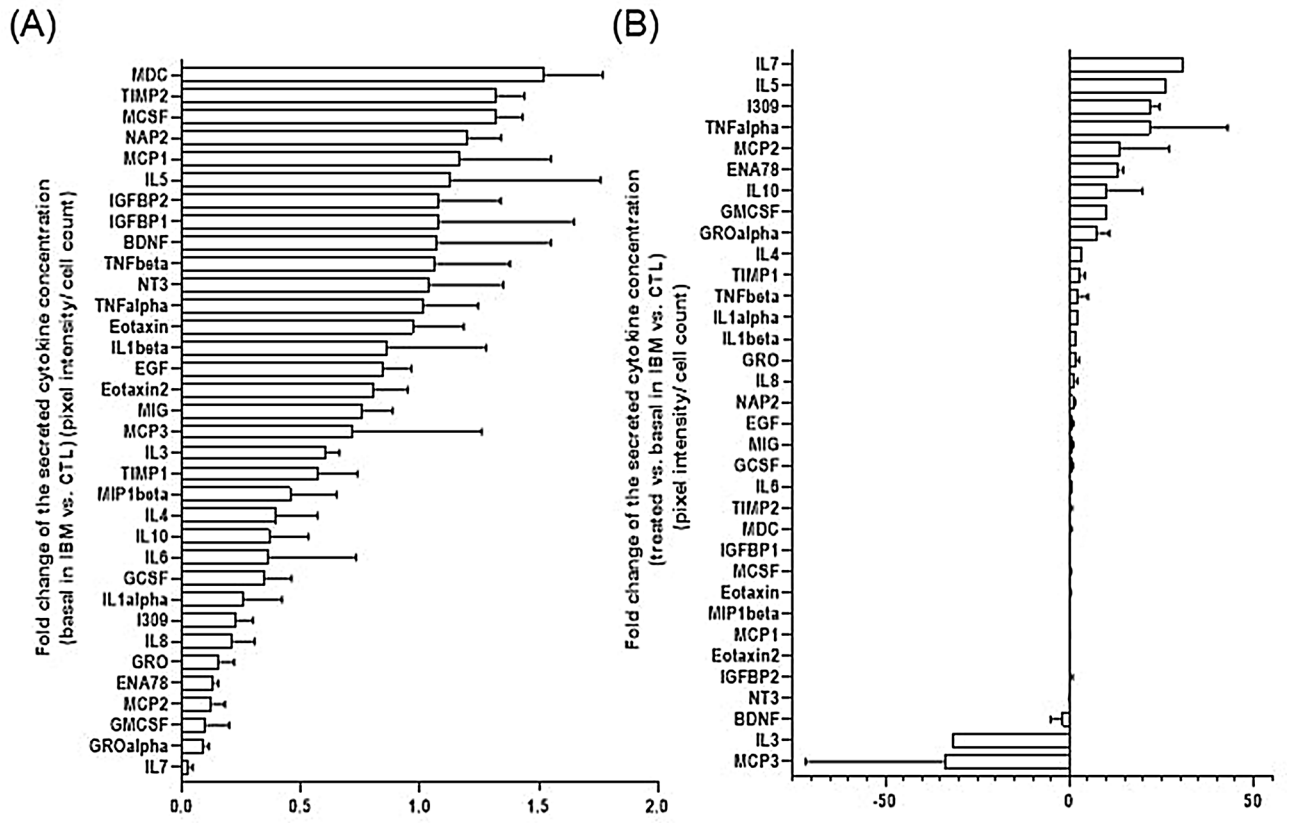

Fig. 6 Secreted cytokines in the supernatant of IBM vs. CTL differentiated myotubes. **A** Fold change of the cytokine concentration in IBM vs. CTL in basal conditions, normalized by cell count. **B** Fold change of the cytokine concentration in treated vs. basal IBM vs. CTLs, normalized by cell count. The secretion of cytokines was overall preserved in basal conditions (**A**) but increased in IBM patients vs. CTLs after LPS exposure (**B**)

Mitochondrial function was altered in IBM vs. CTL iPSC-myotubes

Mitochondrial function was examined by measuring oxygen consumption in mitochondrial respiration and displayed a similar profile in IBM vs. CTL iPSC-myotubes, slightly reduced in the case of CTL (Fig. 8a). Aligned with this, oxidative stress, related to oxygen consumption or reactive oxygen species (ROS) detoxification, was also conserved (TAC levels were preserved) (Fig. 8b). However, we found increased lactate secretion on IBM iPSC-myotubes (Fig. 8b) together with slightly reduced COX activity and consequently, a lower COX/CS ratio (Fig. 8c), highly consistent with mitochondrial disease and histological findings of IBM muscle.

Even though we found no differences in mitochondrial respiration or antioxidant defense, decreased mitochondrial COX/CS activity and increased lactate secretion revealed mitochondrial dysfunction in IBM iPSC-myotubes, resembling IBM features.

Discussion

In this study, the aim was to characterize the IBM iPSC-myotubes model. Despite the inflammatory profile was weak, the rest of the IBM hallmarks were present in this model, reinforcing its value for studying IBM. In this section, we briefly covered some of the benefits and caveats in the development of this model.

Generally, iPSCs for human disease modeling were established for monogenic disorders, with high penetrance, early-onset, and a defined cellular phenotype. On the contrary, in complex disorders, with low penetrance, late onset, or aberrant morphogenesis in target organs, iPSC modeling is more challenging [3]. Successful modeling using iPSCs has been reported in monogenic diseases such as Lesch–Nyhan disease [46] and fragile X syndrome [18], chromosopathies such as Down syndrome [8], and lately, also for complex disorders such as Turner syndrome [25], autism spectrum disorder (ASD) [17] and schizophrenia [7]. Thus, iPSCs may also be promising to model complex diseases, as IBM or other myositis.

The iPSC to muscle cell differentiation approaches are based on growth factors or gene transfection. Our growth factor approach was effective for obtaining functional myotubes in IBM vs. CTL groups within 21 days in culture. However, their survival time as mature myotubes was limited to 7 to 10 days, limiting the accumulation of age-related disturbances. Despite that, we found myopathy-related hallmarks in IBM iPSC-myotubes by mRNA

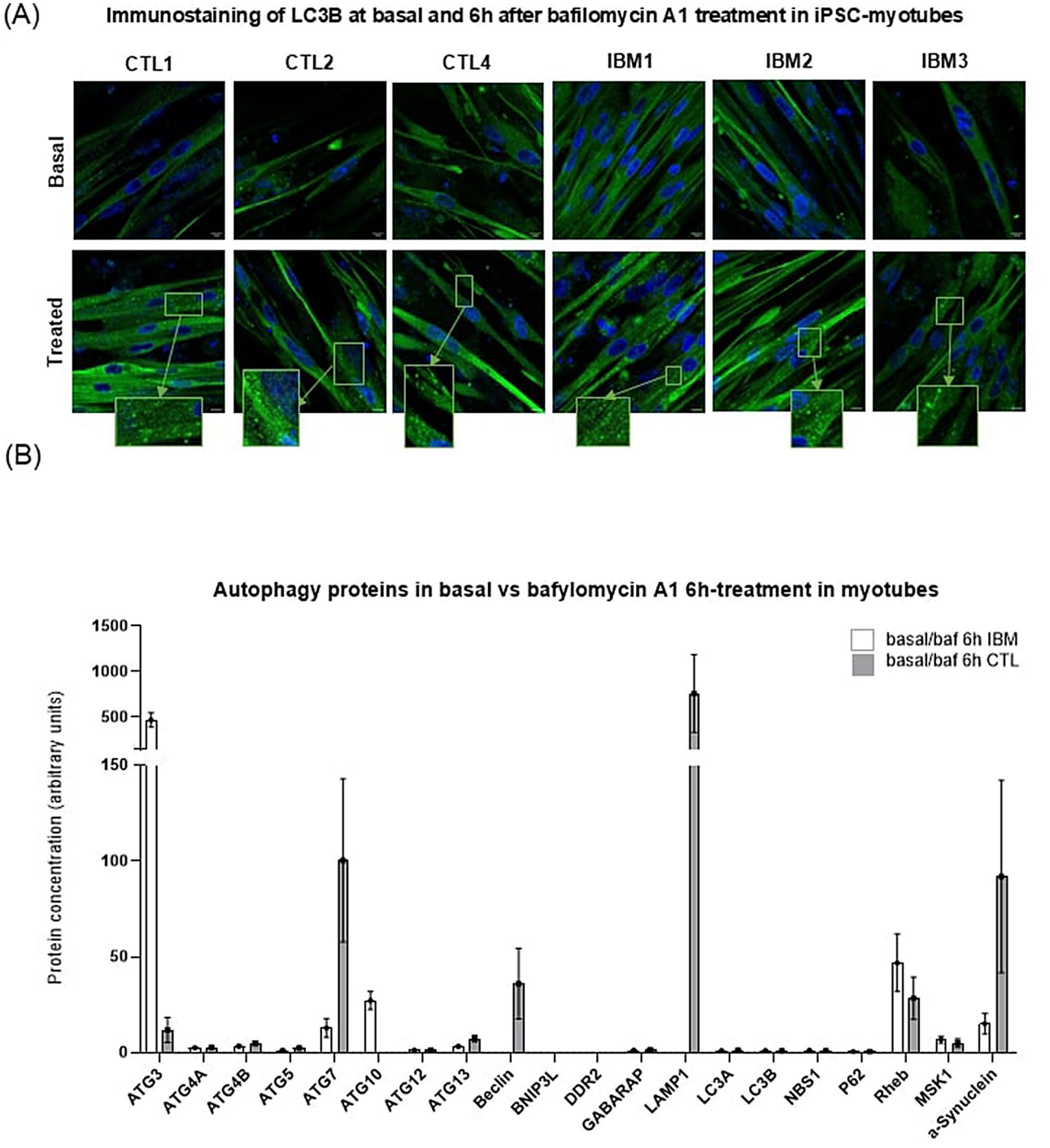

Fig. 7 Autophagy profile in IBM vs. CTL iPSC-derived myotubes. **A** Immunostaining of LC3 autophagosome marker at basal conditions vs. 6 h-bafilomycin A1-treated myotubes. Arrows pointed to the accumulated autophagosomes (green dots). Scale: 10 μM. **B** Autophagy protein concentration in basal vs. bafilomycin A1 treatment in IBM vs. CTLs. Autophagy was less active in IBM iPSC-myotubes than in CTLs, with less production of autophagosomes and autophagy mediators

seq, displaying traits associated to the clinical symptoms, together with inflammatory, autophagic alterations and mitochondrial dysfunction observed at transcriptomic, protein and functional level. Even some authors reported that reprogramming of iPSC could erase the epigenetic marks in patients derived iPSC, as seen with iPSC-derived from diabetes patients [35], in our iPSC-myotubes we found autophagic and mitochondrial alterations in basal conditions, and, under LPS, also higher inflammation. These IBM hallmarks were displayed in

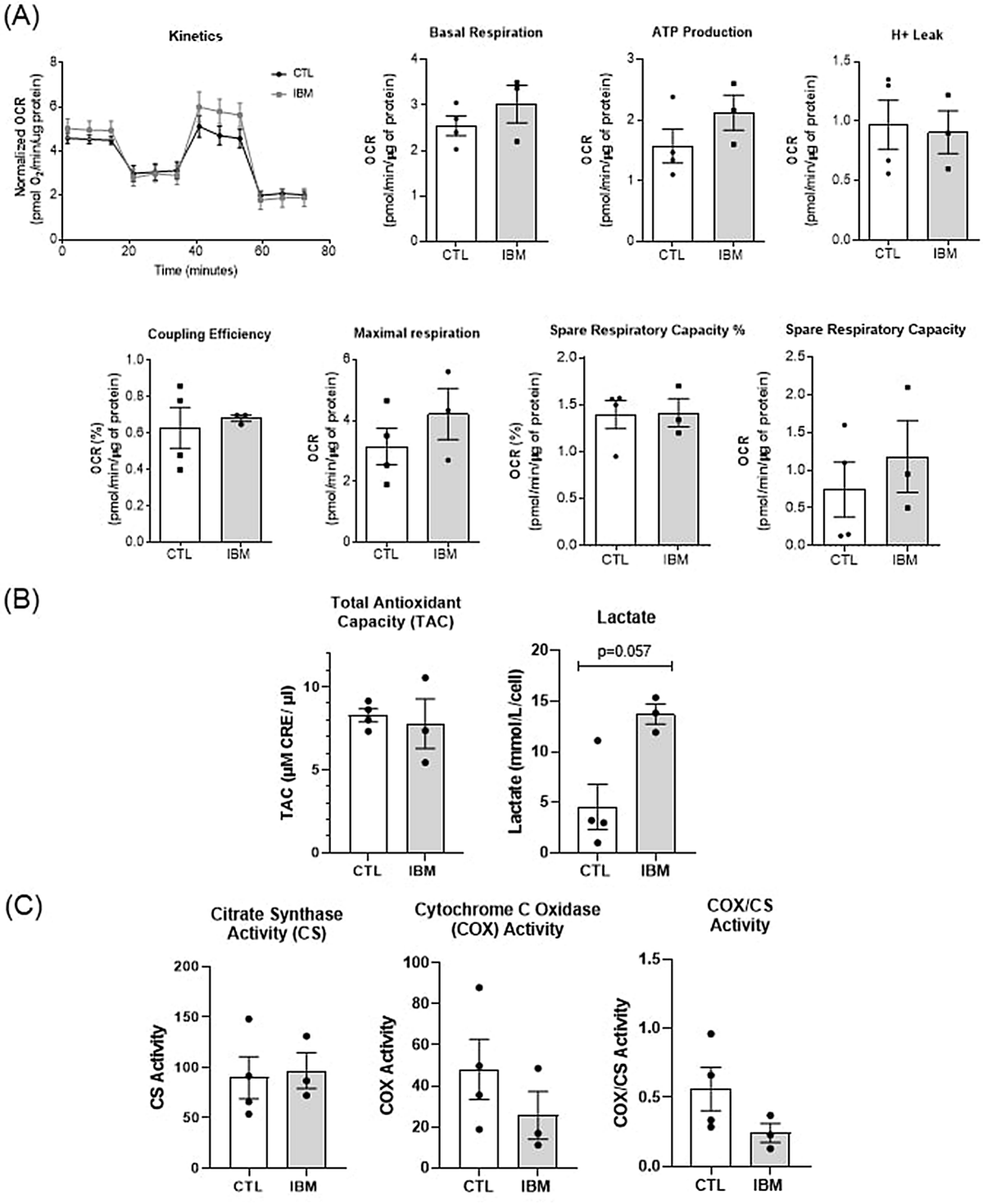

Fig. 8 Mitochondrial profile in IBM vs. CTL iPSC-derived myotubes. **A** Mitochondrial respiration is represented by kinetics, basal respiration, ATP production, H + leak, coupling efficiency, maximal respiration, and spare respiratory capacity in IBM vs. CTLs. **B** Total antioxidant capacity (TAC) and lactate secretion in IBM vs. CTLs. **C** Citrate synthase (CS) activity, cytochrome c oxidase activity (COX) and COX/CS ratio. Mitochondrial respiration and TAC were conserved between cohorts, but lactate and COX/CS were reduced in IBM iPSC-myotubes displaying mitochondrial dysfunction

IBM iPSC-myotubes, in most assays without stressors, suggesting that some genetic, epigenetic or environmental marks that could contribute to disease etiology, would be maintained along the reprogramming [32]. Blood or urine biomarkers of disease support systemic deregulation in IBM [13], beyond muscle involvement, together with the validation of cell models derived from non-target tissues of patients (including fibroblasts [10] and the present iPSC-myotubes).

To validate this model, we combined OMICs and functional analysis. The mRNA seq analysis revealed top DEGs in IBM iPSC-myotubes related to muscle fiber structure, contraction, muscle weakness, autophagic vacuoles and neuromuscular dysphagia. The enrichment analysis displayed GO terms associated with muscle structure, development and differentiation, and HPO terms related to myopathy, including proximal muscle weakness and abnormal muscle fiber morphology. Thus, mRNA seq findings were directly associated with clinical and molecular symptoms in IBM.

Remarkably, inflammation was nearly absent in the mRNA seq. Interestingly, when treated with LPS, IBM iPSC-myotubes displayed a higher inflammatory profile, suggesting susceptibility for immune reactions, and also higher HLA expression, as seen in the muscle of IBM patients.

In autophagy, the lower accumulation of TDP-43 (basal conditions) and other autophagy proteins in IBM vs. CTLs when the process was blocked by bafilomycin A1 suggested that IBM cells may not be synthesizing enough autophagy mediators, eventually blocking the process, as previously described in IBM [10].

In mitochondria, mitochondrial respiration and antioxidant defense appeared mostly adequate, but reduced COX/CS activity in IBM and increased lactate levels uncovered mitochondrial dysfunction. Lower COX/CS activity is one of the key IBM muscle hallmarks and lactate is the molecular and clinical marker of mitochondrial disease, both depicting a dysfunctional mitochondrial function in IBM iPSC-myotubes.

All these findings support patient-derived iPSC-myotubes as a relevant model for IBM, reflecting the main muscle hallmarks, including inflammation, autophagy dysfunction and mitochondrial alterations at transcriptomic, protein and functional levels. In further approaches, iPSC-myotubes may benefit from contact with lymphocytes or other immune cells that may boost the inflammatory profile. Also, since aging is associated to IBM development and has been suggested to play a role in IBM etiology, cell models may also take advantage of promoting aging features by exposure to specific toxins or expressing genes as *progerin*, a truncated version of the *lamin A* protein involved in the Hutchinson–Gilford progeria syndrome [3], which previously recapitulated cellular aging in Parkinson's disease iPSC-derived neurons [29], potentially promoting premature aging hallmarks in IBM iPSC-myotubes. Additional phenotyping of iPSC-myotubes at morphological level, characterizing cell regenerative or differentiation capacity, as well as the mislocalization or malfunction of proteins and subcellular structures in these cells may strength the validity of this cell model for extended uses.

Interestingly, IBM iPSC-myotubes can be used in more complex systems. The application of iPSCs to in vitro disease modeling in various cell types has been widely embraced in the scientific community, as it enables access to invasive tissues through a non-invasive approach [15]. This modelling in now complemented by integration in more complex cell platforms, such as co-cultures or 3D organ "on-a-chip" designs, that facilitate the interconnection of tissues with fluids or other cell types in a physiologically relevant manner [5, 16, 40]. These approaches could bring us closer to achieving more accurate physiological disease models [15], which may be adequate for modeling IBM, and iPSC-derived myotubes could be one of the sources of sample to construct these systems. The differentiation of iPSC generated here to other cell types (like muscle fibroblasts, immune or endothelial cells) could aid in reproducing more physiological muscle microenvironments and their interactions.

The present study has some limitations, including a limited sample size. Despite this is a proof-of-concept study and IBM is a rare disease, next approaches should include bigger cohorts. Consequently, statistically significant differences were hampered due to the reduced sample size, but also to the fact that our measurements were calculated as a single biological result per sample and parameter (the mean of technical replicates), rather than incorporating several repetitions. Despite that, we find a clear phenotype, characterized with a wide variety of technical approaches. Remarkably, the model requires complex handling protocols, time-consuming and expensive experiments [23, 44] that should ideally be simplified by future technological approaches.

Despite those caveats, this study had relevant strengths. For instance, this was the first attempt to model IBM using iPSC-derived myotubes, which reflect some myopathic, inflammatory, autophagic and mitochondrial alterations from this disease. iPSC have unlimited proliferative potential and they could permanently be in a biobank ready to be differentiated into myotubes, to perform large-scale muscle cell platforms for high-throughput screening of therapeutic compounds in IBM. That would be impossible in primary myoblasts, that become senescent after a few rounds of division. In addition, IBM iPSC-myotubes maintain the genetic, epigenetic and environmental cues of affected patients, and can be successfully differentiated into the target tissue of the

disease (or any cell of interest) for construction of more complex and integrated cell systems (including 3D platforms with different cell components). Additionally, deregulated pathways and molecular players depicted while validating this model offer promising avenues for further exploration and may provide novel insights into IBM pathogenesis.

Overall, this proof-of-concept study of IBM iPSC-myotubes revealed that they recapitulated myopathic, inflammatory, autophagic and mitochondrial alterations. Thus, they could be valuable to increase the understanding of IBM pathophysiology, for the identification of biomarkers, and for testing potential treatments.

Conclusions

In summary, IBM is a complex disease with multi-factorial contributors and limited disease models. IBM iPSC-derived myotubes effectively replicated key histopathological features of IBM, including aberrant expression of HLA, TDP-43, and COX markers. mRNA sequencing identified differentially expressed genes (DEGs) associated with myopathy, muscle structure, and developmental changes. Functionally, baseline inflammation was comparable between the IBM and control groups, but it significantly increased in IBM iPSC-myotubes upon lipopolysaccharide treatment. Autophagy was disrupted, with reduced levels of autophagy mediators. Mitochondrial dysfunction was also prominent, characterized by a preserved respiratory profile and antioxidant capacity, but with a decreased cytochrome c oxidase/citrate synthase ratio and elevated lactate secretion. Collectively, these findings highlight patient-derived iPSC-myotubes as a relevant model for IBM, replicating the main muscle hallmarks, including inflammation, autophagy dysfunction, and mitochondrial abnormalities at transcriptomic, protein, and functional levels. As such, this model holds promise for advancing the understanding of IBM pathophysiology, identifying biomarkers, and evaluating potential treatments.

Abbreviations

IBM	Inclusion body myositis
CTL	Healthy volunteer (control)
DEGs	Differentially expressed genes
EBs	Embryoid bodies
LPS	Lipopolysaccharide
MRC	Mitochondrial respiratory chain
TAC	Total antioxidant capacity
COX	Cytochrome c oxidase
CS	Citrate synthase

Supplementary Information

The online version contains supplementary material available at https://doi.org/10.1186/s40478-025-01933-0.

Supplementary Material 1

Supplementary Material 2

Acknowledgements

We acknowledge the contribution of patients and their families, collaborating to expand the state-of-the-art in rare diseases. We also appreciate the support given by the Advanced Optical Microscopy department of the University of Barcelona.

Author contributions

Conceptualization, GG, JCM, AS, JC-S.; methodology, JC-S, LV-R, ET, FJG-G, MG-M, FA-S, AV-C, JP, EP, IM, PS, CG-R, JCF-C, PJM-L, ASO'C; software, AE-C, BM-M, JC-S; validation, GG, AS, JC-S; formal analysis and investigation, GG and JC-S; resources, GG; data curation, GG, JCM, AS, AE-C, BM-M, JC-S; writing—original draft preparation, GG, AS, JC-S; writing—review and editing, all authors; visualization, all authors; supervision, GG and JC-S; funding acquisition, GG. All authors have read and agreed to the published version of the manuscript.

Funding

This study has been funded by Instituto de Salud Carlos III (ISCIII) through the projects PI21/00935 and PI24/00428 and co-funded by the European Union. Additional funding for material and human resources was obtained by the Centro de Investigación Biomédica en Red de Enfermedades Raras (CIBERER), an initiative of the ISCIII and the FEDER. MG-M is supported by CD21/00019 (ISCIII-FSE+), LV-R is supported by FI22/00142 (ISCIII-NextGenerationEU) and A.S. by the grant PID2022-137672NB-I00 (funded by MCIN/AEI/https://doi.org/10.13039/501100011033 and by the ERDF A way of making Europe), the grant PDC 2022-133826-100 (funded by MCIN/AEI/https://doi.org/10.13039/501100011033 and by the European Union Next Generation EU/PRTR), the grant CNS2023-144709 (funded by MCIN/AEI/https://doi.org/10.13039/501100011033 and by the European Union Next Generation EU/PRTR), and the Catalan Government also participated in funding both GG and AS's research groups (2021SGR00453 and 2021-SGR-01423).

Data availability

No datasets were generated or analysed during the current study.

Declarations

Ethics approval and consent to participate

All human studies have been approved by the Ethical Committee of the Hospital Clínic of Barcelona (code HCB/2019/0558), following the ethical standards of the Declaration of Helsinki (1964). Participants signed the corresponding informed consent to enroll in the study.

Consent for publication

Not applicable.

Competing interests

The authors declare no competing interests.

Author details

[1]Inherited Metabolic Diseases and Muscular Disorders Research Group, Department of Internal Medicine, Faculty of Medicine and Health Sciences, Institut d'Investigacions Biomèdiques August Pi i Sunyer (IDIBAPS), Hospital Clinic of Barcelona, University of Barcelona, Barcelona, Spain
[2]CIBERER— Spanish Biomedical Research Centre in Rare Diseases - ISCIII, Madrid, Spain
[3]Centro Nacional de Análisis Genómico, CNAG, Barcelona Institute of Science and Technology, Barcelona, Spain
[4]Universitat Pompeu Fabra (UPF), Barcelona, Spain
[5]Biochemistry and Molecular Genetics Department, Hospital Clinic of Barcelona and Institut d'Investigacions Biomèdiques August Pi I Sunyer (IDIBAPS), Barcelona 08036, Spain
[6]Department of Cell Death and Proliferation, Institute of Biomedical Research of Barcelona (IIBB-CSIC), Liver Unit- HCB-IDIBAPS, Barcelona, Spain
[7]CIBEREHD-Spanish Biomedical Research Centre in Hepatic and Digestive Diseases, Madrid, Spain

[8]Vall d'Hebrón Systemic Autoimmune Diseases Unit. Internal Medicine Service, Hospital Universitari Vall d'Hebrón (HVH), Universitat Autònoma de Barcelona (UAB), Barcelona, Spain
[9]Departament de Biologia Cel·lular, Fisiologia i Immunologia, Facultat de Biologia, Institute of Neuroscience, Universitat de Barcelona, Barcelona, Spain
[10]Institute of Biomedicine (IBUB), University of Barcelona, Barcelona, Spain

Received: 25 November 2024 / Accepted: 23 January 2025
Published online: 21 February 2025

References

1. Ahmed M, Machado PM, Miller A, Spicer C, Herbelin L, He J et al (2016) Targeting protein homeostasis in sporadic inclusion body myositis. Sci Transl Med 8:331–ra41. https://doi.org/10.1126/scitranslmed.aad4583
2. Auburger G, Klinkenberg M, Drost J, Marcus K, Morales-Gordo B, Kunz WS et al (2012) Primary skin fibroblasts as a model of Parkinson's disease. Mol Neurobiol 46:20–27. https://doi.org/10.1007/s12035-012-8245-1
3. Avior Y, Sagi I, Benvenisty N (2016) Pluripotent stem cells in disease modelling and drug discovery. Nat Rev Mol Cell Biol 17:170–182. https://doi.org/10.1038/nrm.2015.27
4. Belinky F, Nativ N, Stelzer G, Zimmerman S, Stein TI, Safran M et al (2015) PathCards: Multi-source consolidation of human biological pathways. Database 2015:1–13. https://doi.org/10.1093/database/bav006
5. Benam KH, Dauth S, Hassell B, Herland A, Jain A, Jang K-J et al (2015) Engineered in vitro disease models. Annu Rev Pathol 10:195–262. https://doi.org/10.1146/annurev-pathol-012414-040418
6. Bordi M, De Cegli R, Testa B, Nixon RA, Ballabio A, Cecconi F (2021) A gene toolbox for monitoring autophagy transcription. Cell Death & Disease 2021 12:11 12:1–7. https://doi.org/10.1038/s41419-021-04121-9
7. Brennand KJ, Simone A, Jou J, Gelboin-Burkhart C, Tran N, Sangar S et al (2011) Modelling schizophrenia using human induced pluripotent stem cells. Nat 2011 473:7346. https://doi.org/10.1038/NATURE09915
8. Briggs JA, Sun J, Shepherd J, Ovchinnikov DA, Chung T-L, Nayler SP et al (2013) Integration-free Induced pluripotent stem cells Model genetic and neural developmental features of Down Syndrome Etiology. Stem Cells 31:467–478. https://doi.org/10.1002/stem.1297
9. Britson KA, Ling JP, Braunstein KE, Montagne JM, Kastenschmidt JM, Wilson A et al (2022) Loss of TDP-43 function and rimmed vacuoles persist after T cell depletion in a xenograft model of sporadic inclusion body myositis. Sci Transl Med 14:9196. https://doi.org/10.1126/scitranslmed.abi9196
10. Cantó-Santos J, Valls-Roca L, Tobías E, García-García FJ, Guitart-Mampel M, Esteve-Codina A et al (2023) Unravelling inclusion body myositis using a patient-derived fibroblast model. J Cachexia Sarcopenia Muscle 14:964–977. https://doi.org/10.1002/jcsm.13178
11. Caron L, Kher D, Lee KL, McKernan R, Dumevska B, Hidalgo A et al (2016) A human pluripotent stem cell model of Facioscapulohumeral muscular dystrophy-affected skeletal muscles. Stem Cells Transl Med 5:1145–1161. https://doi.org/10.5966/sctm.2015-0224
12. Catalán M, Selva-O'Callaghan A, Grau JM (2014) Diagnosis and classification of sporadic inclusion body myositis (sIBM). Autoimmun Rev 13:363–366. https://doi.org/10.1016/j.autrev.2014.01.016
13. Catalán-García M, Oria Garrabou G, Morén C, Guitart-Mampel M, Hernando A et al (2016) Angels Díaz-Ramos `,. Mitochondrial DNA disturbances and deregulated expression of oxidative phosphorylation and mitochondrial fusion proteins in sporadic inclusion body myositis. Clin Sci 130:1741–1751. https://doi.org/10.1042/CS20160080
14. Chal J, Oginuma M, Al Tanoury Z, Gobert B, Sumara O, Hick A et al (2015) Differentiation of pluripotent stem cells to muscle fiber to model Duchenne muscular dystrophy. Nat Biotechnol 33:962–969. https://doi.org/10.1038/nbt.3297
15. Chal J, Al Tanoury Z, Hestin M, Gobert B, Aivio S, Hick A et al (2016) Generation of human muscle fibers and satellite-like cells from human pluripotent stem cells in vitro. Nat Protoc 11:1833–1850. https://doi.org/10.1038/nprot.2016.110
16. Demestre M, Orth M, Föhr KJ, Achberger K, Ludolph AC, Liebau S et al (2015) Formation and characterisation of neuromuscular junctions between hiPSC derived motoneurons and myotubes. Stem Cell Res 15:328–336. https://doi.org/10.1016/J.SCR.2015.07.005
17. DeRosa BA, Van Baaren JM, Dubey GK, Lee JM, Cuccaro ML, Vance JM et al (2012) Derivation of autism spectrum disorder-specific induced pluripotent stem cells from peripheral blood mononuclear cells. Neurosci Lett 516:9. https://doi.org/10.1016/J.NEULET.2012.02.086
18. Eiges R, Urbach A, Malcov M, Frumkin T, Schwartz T, Amit A et al (2007) Developmental Study of Fragile X Syndrome using human embryonic stem cells derived from preimplantation genetically diagnosed embryos. Cell Stem Cell 1:568–577. https://doi.org/10.1016/j.stem.2007.09.001
19. GeneALaCart - GeneCards Batch Queries https://genealacart.genecards.org/. Accessed 28 May 2023
20. GeneTable https://www.musclegenetable.fr/index.html. Accessed 28 May 2023
21. González-Casacuberta I, Juárez-Flores DL, Morén C, Garrabou G (2019) Bioenergetics and Autophagic Imbalance in patients-Derived Cell models of Parkinson Disease supports systemic dysfunction in Neurodegeneration. Front Neurosci 13:1–20. https://doi.org/10.3389/fnins.2019.00894
22. Greenberg SA (2019) Inclusion body myositis: clinical features and pathogenesis. Nat Rev Rheumatol 15:257–272. https://doi.org/10.1038/s41584-019-0186-x
23. Greenberg SA (2020) Pathogenesis of inclusion body myositis. Curr Opin Rheumatol 32:542–547. https://doi.org/10.1097/BOR.0000000000000752
24. Incitti T, Magli A, Magli A, Jenkins A, Lin K, Yamamoto A et al (2020) Pluripotent stem cell-derived skeletal muscle fibers preferentially express myosin heavy-chain isoforms associated with slow and oxidative muscles. Skelet Muscle 10:1–11. https://doi.org/10.1186/s13395-020-00234-5
25. Li W, Wang X, Fan W, Zhao P, Chan Y-C, Chen S et al (2012) Modeling abnormal early development with induced pluripotent stem cells from aneuploid syndromes. Hum Mol Genet 21:32–45. https://doi.org/10.1093/hmg/ddr435
26. Lloyd TE, Mammen AL, Amato AA, Weiss MD, Needham M, Greenberg SA (2014) Evaluation and construction of diagnostic criteria for inclusion body myositis. Neurology 83:426–433. https://doi.org/10.1212/WNL.0000000000000642
27. Lundberg IE, Fujimoto M, Vencovsky J, Aggarwal R, Holmqvist M, Christopher-Stine L et al (2021) Idiopathic inflammatory myopathies. Nat Rev Dis Primers 7:86. https://doi.org/10.1038/s41572-021-00321-x
28. Maffioletti SM, Gerli MFM, Ragazzi M, Dastidar S, Benedetti S, Loperfido M et al (2015) Efficient derivation and inducible differentiation of expandable skeletal myogenic cells from human ES and patient-specific iPS cells. Nat Protoc 10:941–958. https://doi.org/10.1038/nprot.2015.057
29. Miller JD, Ganat YM, Kishinevsky S, Bowman RL, Liu B, Tu EY et al (2013) Human iPSC-based modeling of late-onset disease via progerin-induced aging. Cell Stem Cell 13:691–705. https://doi.org/10.1016/j.stem.2013.11.006
30. Moretti A, Fonteyne L, Giesert F, Hoppmann P, Meier AB, Bozoglu T et al (2020) Somatic gene editing ameliorates skeletal and cardiac muscle failure in pig and human models of Duchenne muscular dystrophy. Nature Medicine 2020 26:2 26:207–214. https://doi.org/10.1038/S41591-019-0738-2
31. Mournetas V, Massouridès E, Dupont JB, Kornobis E, Polvèche H, Jarrige M et al (2021) Myogenesis modelled by human pluripotent stem cells: a multi-omic study of Duchenne myopathy early onset. J Cachexia Sarcopenia Muscle 12:209–232. https://doi.org/10.1002/JCSM.12665
32. Nagy S, Khan A, Machado PM, Houlden H (2023) Inclusion body myositis: from genetics to clinical trials. J Neurol 270:1787–1797. https://doi.org/10.1007/s00415-022-11459-3
33. Nogalska A, D'Agostino C, Engel WK, Askanas V (2014) Sodium phenylbutyrate reverses lysosomal dysfunction and decreases amyloid-β42 in an in vitro-model of inclusion-body myositis. Neurobiol Dis 65:93–101. https://doi.org/10.1016/j.nbd.2014.01.012
34. Ortuño-Costela M, García-López M, Cerrada V, Gallardo ME (2019) < scp > iPSCs: a powerful tool for skeletal muscle tissue engineering. J Cell Mol Med 23:3784–3794. https://doi.org/10.1111/jcmm.14292
35. Pastar I, Marjanovic J, Liang L, Stone RC, Kashpur O, Jozic I et al (2021) Cellular reprogramming of diabetic foot ulcer fibroblasts triggers pro-healing miRNA-mediated epigenetic signature. Exp Dermatol 30:1065–1072. https://doi.org/10.1111/exd.14405
36. PathCards: (2023) Pathways integration. https://pathcards.genecards.org/. Accessed 26 May
37. Perez-Rosendahl M, Mozaffar T (2022) Inclusion body myositis: evolving concepts. Curr Opin Neurol 35:604–610. https://doi.org/10.1097/WCO.0000000000001095
38. Rath S, Sharma R, Gupta R, Ast T, Chan C, Durham TJ et al (2021) MitoCarta3.0: an updated mitochondrial proteome now with sub-organelle localization

and pathway annotations. Nucleic Acids Res 49:D1541–D1547. https://doi.org/10.1093/nar/gkaa1011
39. Schmidt J, Barthel K, Wrede A, Salajegheh M, Bähr M, Dalakas MC (2008) Interrelation of inflammation and APP in sIBM: IL-1β induces accumulation of β-amyloid in skeletal muscle. Brain 131:1228–1240. https://doi.org/10.1093/brain/awn053
40. Shahriyari M, Islam MR, Sakib SM, Rinn M, Rika A, Krüger D et al (2022) Engineered skeletal muscle recapitulates human muscle development, regeneration and dystrophy. J Cachexia Sarcopenia Muscle 13:3106–3121. https://doi.org/10.1002/jcsm.13094
41. Speciale AA, Ellerington R, Goedert T, Rinaldi C (2020) Modelling neuromuscular diseases in the age of Precision Medicine. J Pers Med 10:178. https://doi.org/10.3390/jpm10040178
42. Sugarman MC, Yamasaki TR, Oddo S, Echegoyen JC, Murphy MP, Golde TE et al (2002) Inclusion body myositis-like phenotype induced by transgenic overexpression of βAPP in skeletal muscle. Proc Natl Acad Sci U S A 99:6334–6339. https://doi.org/10.1073/pnas.082545599
43. Szklarczyk D, Kirsch R, Koutrouli M, Nastou K, Mehryary F, Hachilif R et al (2023) The STRING database in 2023: protein-protein association networks and functional enrichment analyses for any sequenced genome of interest. Nucleic Acids Res 51:D638–D646. https://doi.org/10.1093/nar/gkac1000
44. The Human Protein Atlas https://www.proteinatlas.org/. Accessed 29 May 2023
45. Tokuyama T, Hirai A, Shiiba I, Ito N, Matsuno K, Takeda K et al (2020) Mitochondrial dynamics Regulation in skin fibroblasts from mitochondrial disease patients. Biomolecules 10:450. https://doi.org/10.3390/biom10030450
46. Urbach A, Schuldiner M, Benvenisty N (2004) Modeling for Lesch-Nyhan Disease by Gene Targeting in Human Embryonic Stem cells. Stem Cells 22:635–641. https://doi.org/10.1634/stemcells.22-4-635
47. Weihl CC (2019) Sporadic inclusion body myositis and other Rimmed Vacuolar myopathies. CONTINUUM: Lifelong Learn Neurol 25:1586–1598. https://doi.org/10.1212/CON.0000000000000790
48. Winkler M, von Landenberg C, Kappes-Horn K, Neudecker S, Kornblum C, Reimann J (2021) Diagnosis and Clinical Development of sporadic inclusion body myositis and polymyositis with mitochondrial Pathology: a single-Center Retrospective Analysis. J Neuropathol Exp Neurol 80. https://doi.org/10.1093/jnen/nlab101
49. Yi H, Xue L, Guo M-X, Ma J, Zeng Y, Wang W et al (2010) Gene expression atlas for human embryogenesis. FASEB J 24:3341. https://doi.org/10.1096/FJ.10-158782

Publisher's note